EuroIntervention 2021;17:576-583 published online November 2020

One-step anatomic and function testing by cardiac CT versus second-line functional testing in symptomatic patients with coronary artery stenosis: head-to-head comparison of CT-derived fractional flow reserve and myocardial perfusion imaging

Jelmer Westra[1,2], MD; Zehang Li[2], BSc; Laust Dupont Rasmussen[3], MD; Simon Winther[3], MD, PhD; Guanyu Li[2], BSc; Louise Nissen[3], MD, PhD; Steffen E. Petersen[4,5], MSc, MPH, MD, DPHIL; June Anita Ejlersen[6], MD, PhD; Christin Isaksen[7], MD; Lars Christian Gormsen[8], MD, PhD; Grazina Urbonaviciene[7], MD, PhD; Ashkan Eftekhari[1], MD, PhD; Tingwen Weng[9], MD; Xinkai Qu[9], MD, PhD; Hans Erik Bøtker[1], MD, PhD, DMSci; Evald Høj Christiansen[1], MD, PhD; Niels Ramsing Holm[1], MD; Morten Bøttcher[3], MD, PhD; Shengxian Tu[2]*, PhD

1. Department of Cardiology, Aarhus University Hospital, Aarhus, Denmark; 2. School of Biomedical Engineering, Shanghai Jiao Tong University, Shanghai, China; 3. Department of Cardiology, Hospital Unit West Jutland, Herning, Denmark; 4. Barts Heart Centre, Barts Health NHS Trust, London, United Kingdom; 5. William Harvey Research Institute, NIHR Barts Biomedical Research Centre, Queen Mary University of London, London, United Kingdom; 6. Department of Nuclear Medicine, Hospital Unit West Jutland, Herning, Denmark; 7. Department of Radiology, Regional Hospital of Silkeborg, Silkeborg, Denmark; 8. Department of Nuclear Medicine, Aarhus University Hospital, Aarhus, Denmark; 9. Department of Cardiology, Huadong Hospital Affiliated to Fudan University, Shanghai, China

This paper also includes supplementary data published online at: https://eurointervention.pcronline.com/doi/10.4244/EIJ-D-20-00905

KEYWORDS

- fractional flow reserve
- non-invasive imaging
- stable angina

Abstract

Background: CT-QFR is a novel coronary computed tomography angiography (CTA)-based method for on-site evaluation of patients with suspected obstructive coronary artery disease (CAD).

Aims: We aimed to compare the diagnostic performance of CT-QFR with myocardial perfusion scintigraphy (MPS) and cardiovascular magnetic resonance (CMR) as second-line tests in patients with suspected obstructive CAD after coronary CTA.

Methods: A paired analysis of CT-QFR and MPS or CMR, with an invasive FFR-based classification as reference standard was carried out. Symptomatic patients with >50% diameter stenosis on coronary CTA were randomised to MPS or CMR and referred for invasive coronary angiography.

Results: The rate of coronary CTA not feasible for CT-QFR analysis was 17%. Paired patient-level data were available for 118 patients in the MPS group and 113 in the CMR group. Patient-level diagnostic accuracy was better for CT-QFR than for both MPS (82.2% [95% CI: 75.2-89.2] vs 70.3% [95% CI: 62.0-78.7], p=0.029) and CMR (77.0% [95% CI: 69.1-84.9] vs 65.5% [95% CI: 56.6-74.4], p=0.047). Following a positive coronary CTA and with the intention to diagnose, CT-QFR, CMR and MPS were equally suitable as rule-in and rule-out modalities.

Conclusions: The diagnostic performance of CT-QFR as a second-line test was at least similar to MPS and CMR for the evaluation of obstructive CAD in symptomatic patients presenting with ≥50% diameter stenosis on coronary CTA.

**Corresponding author: Room 123, Med-X Research Institute, Shanghai Jiao Tong University, No. 1954, Huashan Road, Shanghai, 200030, China. E-mail: sxtu@sjtu.edu.cn*

SUBMITTED ON 20/07/2020 - REVISION RECEIVED ON 1st 21/09/2020 / 2nd 15/10/2020 / 3rd 07/11/2020 - ACCEPTED ON 12/11/2020

DOI: 10.4244/EIJ-D-20-00905

Abbreviations

CAD	coronary artery disease
CMR	cardiovascular magnetic resonance
CTA	computed tomography angiography
DS	diameter stenosis
FFR	fractional flow reserve
FFR_{CT}	CT-derived fractional flow reserve
ICA	invasive coronary angiography
MPS	myocardial perfusion scintigraphy
QFR	quantitative flow ratio

Introduction

Coronary computed tomography angiography (CTA) has a class I recommendation as a first-line test for diagnosis of obstructive coronary artery disease (CAD) in patients with low to intermediate pre-test risk[1]. Despite an excellent negative predictive value for ruling out obstructive CAD, coronary CTA's positive predictive value remains unsatisfactory. A well-defined downstream diagnostic strategy for patients with suspected obstructive CAD on coronary CTA is currently lacking.

According to the NICE guidelines, CT-derived fractional flow reserve (FFR_{CT}) may be considered in patients with stable chest pain following positive coronary CTA to ensure appropriate referral for invasive investigations[2]. Quantitative flow ratio (QFR) is an alternative method for fast computation of fractional flow reserve (FFR) from coronary images using three-dimensional coronary reconstruction and fluid dynamic equations[3]. A recent pilot study applied the QFR algorithm to coronary CTA (CT-QFR) with promising results[4]. However, CT-QFR has not been compared to perfusion imaging for second-line investigation following coronary CTA indicative of obstructive CAD.

The main aim of the current study was to compare the diagnostic performance of CT-QFR, myocardial perfusion scintigraphy (MPS) and perfusion cardiovascular magnetic resonance (CMR) as second-line tests after a coronary CTA showing at least one vessel with >50% diameter stenosis using an invasive FFR-based classification as reference standard.

Editorial, see page 534

Methods

STUDY POPULATION

The current work is a substudy of the previously reported DanNICAD study. The study design with patient flow and inclusion/exclusion criteria[5], and the main results[6] have been reported previously. In short, 1,675 patients with new-onset symptoms suggestive of CAD were referred for coronary CTA being the recommended first-line test in Denmark. Exclusion criteria included previous percutaneous coronary intervention (PCI)/coronary artery bypass grafting (CABG), contraindication for adenosine and reduced kidney function (eGFR <40 mL/min). Patients were referred for invasive coronary angiography (ICA) if coronary CTA was indicative of obstructive CAD (≥50% diameter stenosis [DS] in ≥1 coronary segment by visual estimation). Prior to ICA, patients were randomised to either MPS or CMR. Of the 1,675 patients referred for CTA, 391 (23.4%) had at least one coronary stenosis >50% DS by CTA. Of these, 301 (76.9%) completed either MPS or CMR and 362 (92.5%) were evaluated by ICA.

Patients with paired ICA and coronary CTA (n=358) were included in the present substudy. We applied substudy-specific exclusion criteria **(Supplementary Appendix 1)**. The study complied with the Declaration of Helsinki and was approved by the local ethics committee. All patients provided informed written consent. The study was registered at ClinicalTrials.gov (Identifier: NCT02264717).

COMPUTED TOMOGRAPHY-DERIVED QUANTITATIVE FLOW RATIO

The CTA acquisition protocol was not optimised for subsequent CT-QFR analysis and has been described in detail previously[5]. Delineation of the coronary lumen was performed semi-automatically using a validated software package (QAngio CT Research Edition version 3.1; Medis Medical Imaging, Leiden, the Netherlands). Lumen contours were subsequently exported into a prototype software package (CtaPlus; Pulse Medical Imaging Technology, Shanghai, China). Details of the computation are provided in **Supplementary Appendix 1**. In short, all the coronary branches were merged into a hierarchical tree structure. Subsequently, the reference lumen was reconstructed assuming no stenosis. Patient-specific resting coronary flow was computed based on the size of the reference lumen and the allometric scaling law **(Supplementary Figure 1)**. Finally, the CT-QFR value at each position of the coronary tree was computed based on a novel method that was adapted from the invasive angiography-based QFR algorithm, using the simulated hyperaemic flow modelled from the resting flow as boundary condition[3]. The coronary CTA segmentation was performed at a core laboratory (CardHemo; Med-X Research Institute, Shanghai Jiao Tong University, Shanghai, China) by experienced analysts, who were blinded to demographic, invasive FFR, and follow-up data. The observer variability at the core laboratory was reported previously[4]. After completing all CT-QFR analyses, the CT-QFR values were transferred to Aarhus University Hospital, Denmark, for statistical analysis. For CT-QFR, ≤0.80 was used as diagnostic cut-off. A fixed CT-QFR value of 0.50 was applied to subocculded and occluded vessels.

MYOCARDIAL PERFUSION IMAGING AND INVASIVE CORONARY ANGIOGRAPHY

The MPS, CMR and ICA protocols are shown in **Supplementary Appendix 1**.

STATISTICAL ANALYSIS

Distribution of data was checked with Q-plots and the Shapiro-Wilk test. Continuous variables are presented as mean±SD, mean (95% CI) or median (IQR) as appropriate. Categorical variables are presented as count (%). Paired diagnostic accuracy, sensitivity

and specificity estimates were compared with McNemar's test. Positive predictive values, negative predictive values and likelihood ratios were compared using generalised score statistics. Diagnostic metrics for CT-QFR, MPS and CMR were recalculated using revascularisation as reference standard. Intention-to-diagnose analysis was performed by classifying non-evaluable and not-performed CT-QFR, MPS and CMR investigations as false-negatives and false-positives according to the ICA/FFR results. Patients and vessels were stratified into four groups based on diagnostic mismatch on a per-patient and per-vessel level. The Breusch-Pagan/Cook-Weisberg test was used to test for per-vessel heteroscedasticity between invasive FFR and CT-QFR. P-values <0.05 were considered significant.

Results

Of 358 patients with paired coronary CTA and ICA, CT-QFR was computed for all vessels in 284 (79%) patients. CT-QFR feasibility accounted for 17% of exclusions, mainly due to motion artefacts and image noise **(Figure 1)**. Patients for whom CT-QFR was not feasible had a higher heart rate and higher Agatston calcium score compared to patients where CT-QFR was feasible **(Supplementary Table 1)**. Complete paired data were available for 118 patients in the MPS group and in 113 patients in the CMR group **(Figure 1)**. Baseline demographics and procedural characteristics are listed in **Table 1** and **Table 2**. A total of 125 (44%) patients had obstructive CAD at ICA with invasive FFR. For vessels with paired assessment of CT-QFR and invasive FFR (n=239), median CT-QFR was 0.87 (IQR: 0.81-0.93) and median invasive FFR was 0.85 (IQR: 0.77-0.90) with 35% of FFR measurements being ≤0.80 **(Supplementary Figure 2)**. The diagnostic performance of CT-QFR is described in **Supplementary Appendix 2**, **Figure 2**, **Table 2**, and **Supplementary Table 2**.

Table 1. Baseline demographics.

Patient characteristics	CT-QFR (n=284)	MPS (n=118)	CMR (n=113)
Demographics			
Age, years	60.7±8.2	60.9±7.8	62.0±7.6
Male	177 (62)	70 (59)	69 (61)
Body mass index, kg/m^2	27.2±4.1	27.2±4.0	27.0±4.0
Risk factors			
Current smoking	55 (19)	25 (21)	16 (14)
Hypertension	193 (68)	80 (68)	78 (69)
Hypercholesterolaemia	98 (35)	36 (31)	37 (33)
Diabetes	25 (9)	5 (4)	11 (10)
Family history of CAD	119 (42)	49 (42)	51 (45)
Symptoms			
Typical angina	88 (31)	38 (32)	33 (29)
Atypical angina	97 (34)	34 (29)	43 (38)
Dyspnoea or arrhythmia	56 (20)	26 (22)	21 (19)
Non-anginal chest pain	43 (15)	20 (17)	16 (14)
Pretest probability of CAD			
Low (<15%)	110 (39)	51 (43)	39 (35)
Intermediate (15%-85%)	174 (61)	67 (57)	74 (65)

Numbers are mean±SD or n (%). CAD: coronary artery disease

COMPARISON OF THE DIAGNOSTIC PERFORMANCE FOR CT-QFR, MPS AND CMR

A comparison of CT-QFR versus MPS and CT-QFR versus CMR on diagnostic performance estimates is presented in **Table 3**, with examples shown in **Figure 3**. While CT-QFR displayed better sensitivity and diagnostic accuracy, specificity was similar between the respective modalities. Based on the likelihood ratios presented in **Table 3**, CT-QFR, CMR and MPS were equally suitable to rule

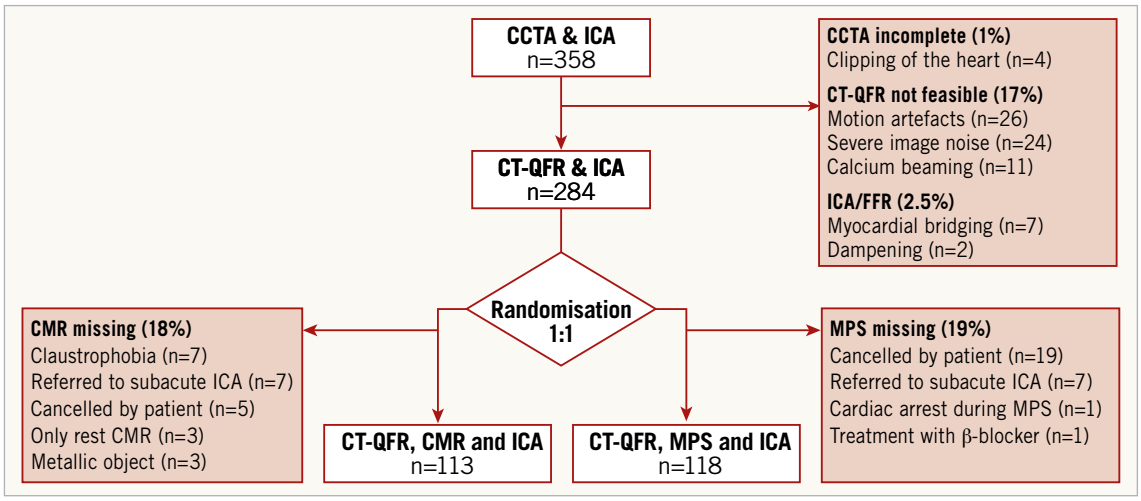

Figure 1. *Study flow chart. CCTA: coronary computed tomography angiography; CMR: cardiovascular magnetic resonance; CT-QFR: CT-derived quantitative flow ratio; FFR: fractional flow reserve; ICA: invasive coronary angiography; MPS: myocardial perfusion scintigraphy*

Table 2. Procedural characteristics.

CCTA and CT-QFR (n=284)		
CCTA		
Heart rate, beats/min		56±7
Agatston score		214 (63-585)
0		22 (8)
1-399		164 (58)
≥400		97 (34)
CT-QFR		
Median (IQR)*		0.85 (0.70-0.91)
≤0.80		107 (38)
0.75-0.85		70 (25)
Fixed 0.50		35 (12)
CMR (n=113)		
Perfusion defects	Reversible	25 (22)
	Mixed	3 (3)
MPS (n=118)		
Perfusion defects	Reversible	15 (13)
	Mixed	8 (6)
	Irreversible	2 (2)
ICA-FFR (n=284)		
Haemodynamic disease	≥1 vessel with FFR ≤0.80	62 (22)
	≥1 vessel with >90% DS	52 (18)
	≥1 vessel with >50% DS QCA	11 (4)

Numbers are mean±SD, mean (IQR) or n (%). *Without fixed CT-QFR values of 0.50. CCTA: coronary computed tomography angiography; CMR: cardiovascular magnetic resonance; CT-QFR: CT-derived quantitative flow ratio; DS: diameter stenosis; FFR: fractional flow reserve; ICA: invasive coronary angiography; IQR: interquartile range; QCA: quantitative coronary angiography

in CAD as defined by ICA and invasive FFR, while CT-QFR was more suitable as a rule-out modality. The same was true with the use of revascularisation as reference standard **(Supplementary Table 3)**. The diagnostic performance estimates for MPS with abnormality defined as a summed stress score (SSS) >3 are presented in **Supplementary Table 4**. When compared to patients with reversible perfusion defects, patients with fixed or irreversible perfusion defects were more likely to have high-grade stenoses as identified by ICA, albeit not reaching statistical significance (46% vs 28%, p=0.18) **(Supplementary Table 5)**.

COMPARISON OF THE DIAGNOSTIC PERFORMANCE FOR CT-QFR, MPS AND CMR WITH THE INTENTION TO DIAGNOSE

An intention-to-diagnose analysis using the full population with conclusive ICA results is presented in **Supplementary Table 6** with 3*2 contingency tables and in **Supplementary Table 7** with diagnostic performance estimates. Sensitivity remained better for CT-QFR when compared to MPS and CMR. Specificity was better for MPS when compared to CT-QFR and similar for CT-QFR when compared to CMR. CT-QFR, MPS and CMR remained equally suitable as rule-in and rule-out modalities **(Supplementary Table 7)**.

Discussion

The main findings were that, following a coronary CTA with suspected obstructive CAD, 1) CT-QFR can be used to rule in and rule out the presence of obstructive epicardial CAD with at least similar efficiency to MPS and CMR, and 2) CT-QFR feasibility was hampered in patients with a high heart rate and high Agatston calcium score.

COMPARISON TO ALTERNATIVE CORONARY CTA-DERIVED FFR SOLUTIONS

Increasing emphasis is given to post-processing of coronary CTA data for derivation of FFR. The pioneer modality, FFR_{CT} (HeartFlow, Redwood City, CA, USA), has good diagnostic accuracy with invasive FFR as reference standard and is able to differentiate high-risk and low-risk patients in terms of deferral or referral to further downstream testing[7,8]. Despite a numerically

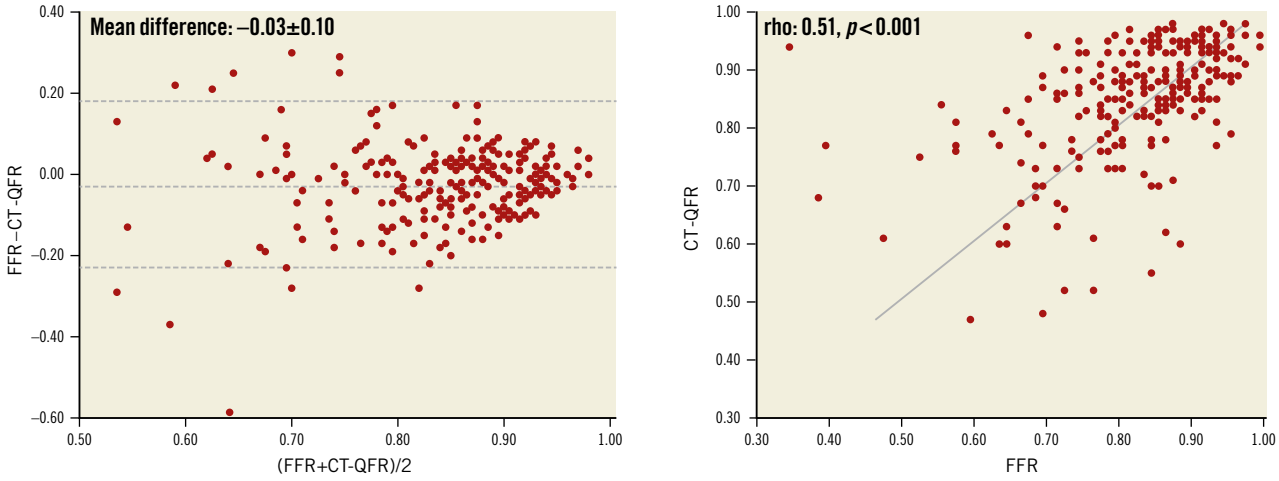

Figure 2. *Lesion-level correlation and agreement of CT-QFR and FFR. CT-QFR: CT-derived quantitative flow ratio; FFR: fractional flow reserve*

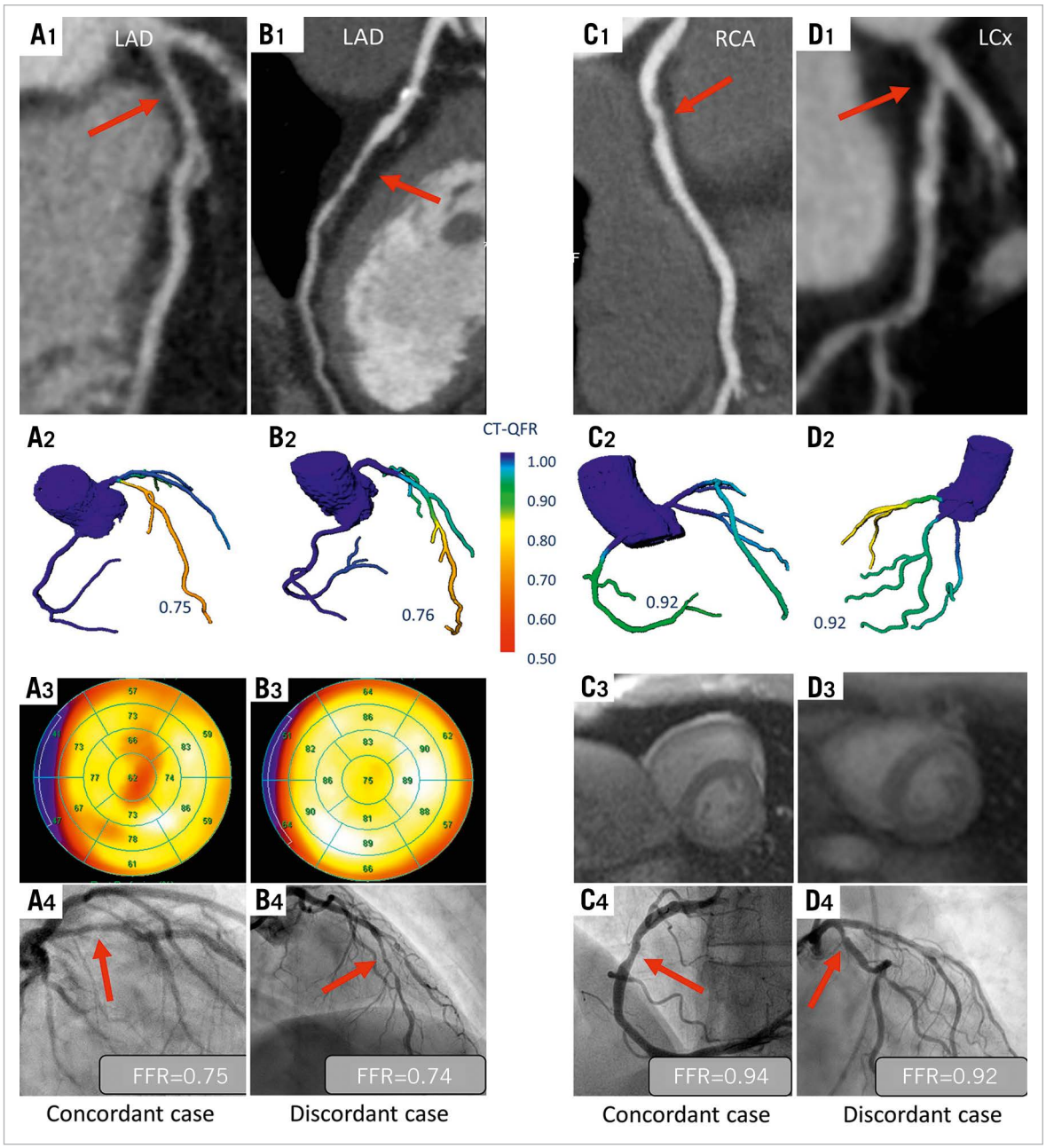

Figure 3. *Illustrative examples of four study patients. A1-A4 indicate coronary CTA-identified intermediate stenosis on the LAD (A1) considered obstructive by CT-QFR (A2), MPS (A3) and invasive FFR (A4). B1-B4 indicate calcified and soft plaques on coronary CTA (B1) considered obstructive by CT-QFR (B2) and invasive FFR (B4) but not by MPS (B3). C1-C4 indicate coronary CTA-identified intermediate stenosis on the RCA (C1) not considered obstructive by CT-QFR (C2), CMR (C3) and invasive FFR (C4). D1-D4 indicate plaques on coronary CTA (D1) not considered obstructive by CT-QFR (D2) and invasive FFR (D4) but obstructive by CMR (D3). CT-QFR: CT-derived quantitative flow ratio; FFR: fractional flow reserve; ICA: invasive coronary angiography; LAD: left anterior descending artery; LCx: left circumflex artery; RCA: right coronary artery*

slightly poorer sensitivity of CT-QFR indicated by this study, the overall diagnostic accuracy of CT-QFR to predict revascularisation appears at least similar to that of FFR_{CT} in a cohort identical to the present analysis (diagnostic accuracy 75.2% for CT-QFR **[Supplementary Table 2]** and 61% for FFR_{CT})[9].

Comparing the presented diagnostic performance estimates to similar studies should be done with caution given the impact of differences in distribution of the target condition (e.g., FFR ≤0.80) and level of calcification that varies substantially[8,10]. The observed per-vessel numerical agreement between CT-QFR and invasive FFR was modest and comparable to other coronary CTA-derived FFR solutions with broad ranges of agreement[11]. The uncertainty related to the numerical agreement indicates that, even though CT-QFR and alternative coronary CTA-derived FFR solutions

Table 3. Comparison of diagnostic performance estimates for CMR versus CT-QFR and MPS versus CT-QFR.

	CT-QFR (n=284)	CMR vs CT-QFR (n=113)			MPS vs CT-QFR (n=118)		
		CMR	CT-QFR	*p*-value	MPS	CT-QFR	*p*-value
Accuracy	80.0 (74.8-84.3)	65.5 (56.6-74.4)	77.0 (69.1-84.9)	0.047	70.3 (62.0-78.7)	82.2 (75.2-89.2)	0.029
Sensitivity	69.6 (60.7-77.5)	37.8 (23.8-53.5)	60.0 (44.3-74.3)	0.053	39.6 (25.8-54.7)	77.1 (62.7-88.0)	<0.001
Specificity	87.4 (81.2-92.1)	83.8 (72.9-91.6)	88.2 (78.1-94.8)	0.607	91.4 (82.3-96.8)	85.7 (75.3-92.9)	0.455
PPV	81.3 (72.6-88.2)	60.7 (40.6-78.5)	77.1 (59.9-89.6)	0.100	76.0 (54.9-90.6)	78.7 (64.3-89.3)	0.778
NPV	78.5 (71.7-84.3)	67.1 (56.0-76.9)	76.9 (66.0-85.7)	0.022	68.8 (58.4-78.0)	84.5 (74.0-92.0)	0.062
LR (+)	5.53 (3.61-8.47)	2.34 (1.21-4.51)	5.10 (2.55-10.20)	0.095	4.62 (1.99-10.71)	5.40 (2.98-9.77)	0.774
LR (–)	0.35 (0.27-0.46)	0.74 (0.58-0.95)	0.45 (0.31-0.66)	0.025	0.66 (0.52-0.84)	0.27 (0.16-0.45)	<0.001
AUC	0.86 (0.82-0.90)	–	–	–	–	–	–

Numbers are mean (95% CI). AUC: area under the receiver operating curve; CMR: cardiovascular magnetic resonance; CT-QFR: CT-derived quantitative flow ratio; LR (–): negative likelihood ratio; LR (+): positive likelihood ratio; NPV: negative predictive value; PPV: positive predictive value

may improve the usual-care diagnostic pathway in patients with suspected obstructive CAD, the numerical value can currently not be used to plan subsequent revascularisation[12].

FFR_{CT} requires transfer of images to a centralised core laboratory. Importantly, a pilot study on CT-QFR using off-the-shelf computers showed that the average segmentation process took 17 minutes, while the subsequent CT-QFR computation on average took 19 seconds, thus illustrating the feasibility and potential for use of CT-QFR in same-day diagnostic work-ups[4]. The latter study found a better correlation and agreement of CT-QFR with FFR compared to our findings. This may be due to several factors. The diagnostic performance estimates may have been affected by retrospective selection of coronary CTA data in the pilot study, while the correlation and agreement may differ because the present study included more severe lesions (FFR <0.60) where the CT-QFR versus FFR scatter was larger.

COMPARISON TO CMR AND MPS

We found a sensitivity of MPS comparable to that reported in a previous study where MPS was tested as second-line modality[13]. Studies of CMR as a second-line test with invasive FFR endpoints are scarce. Studies testing CMR or MPS as first-line test with an FFR-based endpoint generally find sensitivities in the range of 57-90%[14,15]. The low sensitivity in the current report may be explained by the coronary CTA-based referral to MPS and CMR, because high-risk patients (e.g., suspicion of high coronary artery calcium score [CACS], high body mass index [BMI], kidney disease) are generally not referred to coronary CTA. This is backed by the findings of ReASSESS where symptomatic patients were referred to MPS based on 40-90% DS on coronary CTA and where MPS had a sensitivity of 41% (29-55) using an FFR-based reference standard[13].

CT-QFR and invasive FFR are restricted to evaluation of epicardial vasculature, while CMR and MPS also include perfusion of the microvasculature. Hence, a good agreement between CT-QFR and invasive FFR was expected. Despite the fact that abnormal CMR/MPS investigations predominantly counted reversible and mixed perfusion defects **(Table 2)**, our applied definition of abnormal CMR and MPS also included irreversible perfusion defects potentially indicative of infarcts. Irreversible perfusion defects would not be expected to correlate well with a pure FFR-based endpoint. However, the included population did not have any known coronary artery disease upon enrolment and, reflecting routine clinical practice, ICA would be indicated.

It cannot be ruled out that our inclusion of a proportion of patients with atypical symptoms influenced the diagnostic performance estimates, because the sensitivity of perfusion imaging as second-line test after coronary CTA is highest in patients with typical angina, probably due to a higher pre-test risk of obstructive CAD in these patients compared to, e.g., atypical, lower-risk patients[16]. We observed a similar pattern for CT-QFR as sensitivity and diagnostic performance were highest for patients with typical angina and lowest for patients with non-anginal chest pain **(Supplementary Table 2, Supplementary Figure 3)**.

CHALLENGES IN DERIVING FFR FROM CORONARY CTA

The acquisition protocol for coronary CTA in the Dan-NICAD trial did not specify specific standards required for CT-QFR analysis. We found that 17% of the coronary CTA data in Dan-NICAD did not have the required quality for CT-QFR calculation. This is slightly higher compared to previous studies on CT-FFR reporting rejection rates around 12-13%. However, it is in line with FFR_{CT} by HeartFlow when applied to the CMR population from the Dan-NICAD data set (rejection rate 21%)[9]. Coronary calcification was shown to be a particular challenge. Calcium score tended to be higher in patients with false-positive CT-QFR measurements compared to patients with true-negative CT-QFR measurements **(Supplementary Table 3)**. This influence could be caused by challenges related to lumen segmentation in calcified vessels. We included patients prospectively before the knowledge of CTA findings and without specific criteria for CTA quality, which may explain the relatively large total calcium burden (mean total calcium score of 424±424 in the current study compared with, e.g., 302±468 in the Coronary Blood Flow Using CT Angiography: Next Steps [NXT] trial)[8].

Discordant classification was, as expected, more frequent in the CT-QFR range of 0.75-0.85 **(Supplementary Table 7)**. Some natural variance will be present close to the discrimination point for any test with a binary cut-off. Identification of a strict low (refer) and high (defer) CT-QFR limit may ensure a suitable second-line CT-QFR-based strategy following a positive coronary CTA and should be investigated in a prospective manner. Finally, our data indicate that CAD located in the LM and proximal LAD often occurs in vessels with false-negative CT-QFR measurements **(Supplementary Table 7)**. This may reflect challenges of generalised computation algorithms to account for large increases in coronary blood flow, as expected in vessels supplying a large mass of myocardium. Given the prognostic importance of the left main coronary artery (LM) and proximal left anterior descending coronary artery (LAD) lesions, further refinement of the CT-QFR technique could be needed. Application of the QFR algorithm to ICA with the use of a Thrombolysis In Myocardial Infarction (TIMI) frame count yielded better diagnostic performance in previous studies and may therefore reflect a more patient-tailored solution than when using generic flow assumptions such as those in the current report[3].

Limitations

The current Dan-NICAD substudy did not include a specific power calculation for the current aim. Consequently, the study should be considered exploratory and the findings hypothesis-generating. Secondly, the low sensitivity of MPS and CMR may be explained by our applied criteria for abnormal perfusion resulting in many false negatives. However, recalculation of perfusion defects with less stringent criteria provided similar diagnostic performance estimates as illustrated with MPS **(Supplementary Table 3)**. Thirdly, referral of patients to ICA based on a coronary CTA with suspected obstructive CAD may have biased the analysis in favour of CT-QFR. However, coronary CTA is the recommended first-line test and, given the high negative predictive value, it would not be clinically feasible to refer all patients for ICA. Lastly, a substantial number of coronary CTA scans did not meet the criteria for CT-QFR analysis, which may have biased the primary paired CT-FFR versus MPS and CT-QFR versus CMR analyses. Furthermore, CT-QFR was not attempted in vessels with myocardial bridging. However, the intention-to-diagnose analysis likewise revealed that CT-QFR was able to rule in and rule out the presence of obstructive CAD to the same degree as MPS and CMR. Importantly, insufficient coronary CTA quality for CT-QFR analysis can swiftly be identified because the technique does not require transfer of images to a centralised laboratory. The true feasibility rate and time to CT-QFR should be assessed in prospective studies with coronary CTA protocols optimised for post-processing activities.

Conclusions

The diagnostic performance of CT-QFR was at least similar to MPS and CMR for the evaluation of obstructive coronary artery disease in symptomatic patients presenting with ≥50% diameter stenosis on coronary CTA.

Impact on daily practice

The present study found that CT-QFR has a diagnostic performance comparable to MPS and CMR when used as second-line test after coronary CTA with suspected obstructive CAD but with room for improvement in feasibility. Pending confirmation in prospective studies, CT-QFR bears the potential to reduce unnecessary downstream diagnostic procedures and ensure a more appropriate referral of patients for invasive coronary angiography with the aim of identifying obstructive coronary artery disease.

Acknowledgements

S. Tu would like to acknowledge support from the Natural Science Foundation of China (Grant No. 81871460), the Shanghai Municipal Science and Technology Commission (Grant No. 19441913600), and the Program of Shanghai Technology Research Leader. J. Westra acknowledges support from Aarhus University (PhD scholarship). S. Petersen acknowledges support from the National Institute for Health Research Barts Biomedical Research Centre.

Conflict of interest statement

S. Petersen reports personal fees from and is a shareholder of Circle Cardiovascular Imaging, Calgary, Alberta, Canada. There were no direct fees related to this research project. S. Tu reports grants from Pulse Medical Imaging Technology, and Medis Medical Imaging, during the conduct of the study. The other authors have no conflicts of interest to declare.

References

1. Knuuti J, Wijns W, Saraste A, Capodanno D, Barbato E, Funck-Brentano C, Prescott E, Storey RF, Deaton C, Cuisset T, Agewall S, Dickstein K, Edvardsen T, Escaned J, Gersh BJ, Svitil P, Gilard M, Hasdai D, Hatala R, Mahfoud F, Masip J, Muneretto C, Valgimigli M, Achenbach S, Bax JJ; ESC Scientific Document Group. 2019 ESC Guidelines for the diagnosis and management of chronic coronary syndromes. *Eur Heart J.* 2020;41:407-77.

2. National Institute for Health and Care Excellence: Chest pain. [CG95]. 2016. Available at: https://www.nice.org.uk/guidance/cg95

3. Tu S, Westra J, Yang J, von Birgelen C, Ferrara A, Pellicano M, Nef H, Tebaldi M, Murasato Y, Lansky A, Barbato E, van der Heijden LC, Reiber JH, Holm NR, Wijns W; FAVOR Pilot Trial Study Group. Diagnostic Accuracy of Fast Computational Approaches to Derive Fractional Flow Reserve From Diagnostic Coronary Angiography: The International Multicenter FAVOR Pilot Study. *JACC Cardiovasc Interv.* 2016;9:2024-35.

4. Tu S, Westra J, Adjedj J, Ding D, Liang F, Xu B, Holm NR, Reiber JHC, Wijns W. Fractional flow reserve in clinical practice: from wire-based invasive measurement to image-based computation. *Eur Heart J.* 2020;41:3271-9.

5. Nissen L, Winther S, Isaksen C, Ejlersen JA, Brix L, Urbonaviciene G, Frost L, Madsen LH, Knudsen LL, Schmidt SE, Holm NR, Maeng M, Nyegaard M, Botker HE, Bottcher M. Danish study of Non-Invasive testing in Coronary Artery Disease (Dan-NICAD): study protocol for a randomised controlled trial. *Trials.* 2016;17:262.

6. Nissen L, Winther S, Westra J, Ejlersen JA, Isaksen C, Rossi A, Holm NR, Urbonaviciene G, Gormsen LC, Madsen LH, Christiansen EH, Maeng M, Knudsen LL, Frost L, Brix L, Botker HE, Petersen SE, Bottcher M. Diagnosing coronary artery disease after a positive coronary computed tomography angiography: the Dan-NICAD open label, parallel, head to head, randomized controlled diagnostic accuracy trial of cardiovascular magnetic resonance and myocardial perfusion scintigraphy. *Eur Heart J Cardiovasc Imaging.* 2018;19:369-77.

7. Norgaard BL, Terkelsen CJ, Mathiassen ON, Grove EL, Botker HE, Parner E, Leipsic J, Steffensen FH, Riis AH, Pedersen K, Christiansen EH, Maeng M, Krusell LR,

Kristensen SD, Eftekhari A, Jakobsen L, Jensen JM. Coronary CT Angiographic and Flow Reserve-Guided Management of Patients With Stable Ischemic Heart Disease. *J Am Coll Cardiol.* 2018;72:2123-34.

8. Norgaard BL, Leipsic J, Gaur S, Seneviratne S, Ko BS, Ito H, Jensen JM, Mauri L, De Bruyne B, Bezerra H, Osawa K, Marwan M, Naber C, Erglis A, Park SJ, Christiansen EH, Kaltoft A, Lassen JF, Botker HE, Achenbach S; NXT Trial Study Group. Diagnostic performance of noninvasive fractional flow reserve derived from coronary computed tomography angiography in suspected coronary artery disease: the NXT trial (Analysis of Coronary Blood Flow Using CT Angiography: Next Steps). *J Am Coll Cardiol.* 2014;63:1145-55.

9. Ronnow Sand NP, Nissen L, Winther S, Petersen SE, Westra J, Christiansen EH, Larsen P, Holm NR, Isaksen C, Urbonaviciene G, Deibjerg L, Husain M, Thomsen KK, Rohold A, Botker HE, Bottcher M. Prediction of Coronary Revascularization in Stable Angina: Comparison of FFR_{CT} With CMR Stress Perfusion Imaging. *JACC Cardiovasc Imaging.* 2020;13:994-1004.

10. Min JK, Leipsic J, Pencina MJ, Berman DS, Koo BK, van Mieghem C, Erglis A, Lin FY, Dunning AM, Apruzzese P, Budoff MJ, Cole JH, Jaffer FA, Leon MB, Malpeso J, Mancini GB, Park SJ, Schwartz RS, Shaw LJ, Mauri L. Diagnostic accuracy of fractional flow reserve from anatomic CT angiography. *JAMA.* 2012;308:1237-45.

11. Coenen A, Kim YH, Kruk M, Tesche C, De Geer J, Kurata A, Lubbers ML, Daemen J, Itu L, Rapaka S, Sharma P, Schwemmer C, Persson A, Schoepf UJ, Kepka C, Hyun Yang D, Nieman K. Diagnostic Accuracy of a Machine-Learning Approach to Coronary Computed Tomographic Angiography-Based Fractional Flow Reserve: Result From the MACHINE Consortium. *Circ Cardiovasc Imaging.* 2018;11:e007217.

12. Cook CM, Petraco R, Shun-Shin MJ, Ahmad Y, Nijjer S, Al-Lamee R, Kikuta Y, Shiono Y, Mayet J, Francis DP, Sen S, Davies JE. Diagnostic accuracy of computed tomography-derived fractional flow reserve: A systematic review. *JAMA Cardiol.* 2017;2:803-10.

13. Sand NPR, Veien KT, Nielsen SS, Norgaard BL, Larsen P, Johansen A, Hess S, Deibjerg L, Husain M, Junker A, Thomsen KK, Rohold A, Jensen LO. Prospective Comparison of FFR Derived From Coronary CT Angiography With SPECT Perfusion Imaging in Stable Coronary Artery Disease: The ReASSESS Study. *JACC Cardiovasc Imaging.* 2018;11:1640-50.

14. Danad I, Szymonifka J, Twisk JWR, Norgaard BL, Zarins CK, Knaapen P, Min JK. Diagnostic performance of cardiac imaging methods to diagnose ischaemia-causing coronary artery disease when directly compared with fractional flow reserve as a reference standard: a meta-analysis. *Eur Heart J.* 2017;38:991-8.

15. Danad I, Raijmakers PG, Driessen RS, Leipsic J, Raju R, Naoum C, Knuuti J, Maki M, Underwood RS, Min JK, Elmore K, Stuijfzand WJ, van Royen N, Tulevski II, Somsen AG, Huisman MC, van Lingen AA, Heymans MW, van de Ven PM, van Kuijk C, Lammertsma AA, van Rossum AC, Knaapen P. Comparison of Coronary CT Angiography, SPECT, PET, and Hybrid Imaging for Diagnosis of Ischemic Heart Disease Determined by Fractional Flow Reserve. *JAMA Cardiol.* 2017;2:1100-7.

16. Nissen L, Winther S, Westra J, Ejlersen JA, Isaksen C, Rossi A, Holm NR, Urbonaviciene G, Gormsen LC, Madsen LH, Christiansen EH, Maeng M, Knudsen LL, Frost L, Brix L, Bøtker HE, Petersen SE, Bøttcher M. Influence of Cardiac CT based disease severity and clinical symptoms on the diagnostic performance of myocardial perfusion. *Int J Cardiovasc Imaging.* 2019;35:1709-20.

17. Hachamovitch R, Berman DS, Shaw LJ, Kiat H, Cohen I, Cabico JA, Friedman J, Diamond GA. Incremental prognostic value of myocardial perfusion single photon emission computed tomography for the prediction of cardiac death: differential stratification for risk of cardiac death and myocardial infarction. *Circulation.* 1998;97:535-43.

18. Choy JS, Kassab GS. Scaling of myocardial mass to flow and morphometry of coronary arteries. *J Appl Physiol (1985).* 2008;104:1281-6.

19. West GB, Brown JH, Enquist BJ. A general model for the origin of allometric scaling laws in biology. *Science.* 1997;276:122-6.

20. Tu S, Barbato E, Köszegi Z, Yang J, Sun Z, Holm NR, Tar B, Li Y, Rusinaru D, Wijns W, Reiber JH. Fractional flow reserve calculation from 3-dimensional quantitative coronary angiography and TIMI frame count: a fast computer model to quantify the functional significance of moderately obstructed coronary arteries. *JACC Cardiovasc Interv.* 2014;7:768-77.

21. Huo Y, Finet G, Lefèvre T, Louvard Y, Moussa I, Kassab GS. Optimal diameter of diseased bifurcation segment: a practical rule for percutaneous coronary intervention. *EuroIntervention.* 2012;7:1310-6.

Supplementary data

Supplementary Appendix 1. Methods.

Supplementary Appendix 2. Results.

Supplementary Figure 1. A normal bifurcation model.

Supplementary Figure 2. Distribution of CT-QFR and FFR on a per-vessel level.

Supplementary Figure 3. Diagnostic performance of CT-QFR stratified by symptoms.

Supplementary Table 1. Comparison of clinical and procedural characteristics stratified by CT-QFR feasibility.

Supplementary Table 2. Mismatch characteristics.

Supplementary Table 3. Diagnostic performance using revascularisation as reference standard.

Supplementary Table 4. Diagnostic performance of MPS using SSS >3 as criteria for abnormality.

Supplementary Table 5. Haemodynamic obstructive disease stratified by type of perfusion defect.

Supplementary Table 6. Patient level 3*2 contingency tables with the intention to diagnose.

Supplementary Table 7. Diagnostic performance with the intention to diagnose.

The supplementary data are published online at: https://eurointervention.pcronline.com/doi/10.4244/EIJ-D-20-00905

Supplementary data

Supplementary Appendix 1. Methods

Study population

We applied substudy-specific exclusion criteria: I) clipping of CTA images not visualising the whole heart; II) poor CTA image quality due to strong image noise; III) severe artefacts precluding CT-QFR computation, including motion artefacts and calcium beaming artefacts; IV) perfusion imaging not performed; V) presence of a myocardial bridging in the interrogated vessels; and VI) dampening of the invasive pressure pullback curves. Revascularisation was based on ICA and invasive FFR using ≤0.80 as cut-off for invasive FFR. Physicians responsible for downstream patient management including revascularisation were blinded to the results of the myocardial perfusion imaging. Patients with paired CT-QFR, CMR and ICA (n=113) or paired CT-QFR, MPS and ICA (n=118) constituted the population for the primary diagnostic comparison **(Figure 1)**. Patients with successful CT-QFR computation of all vessels (n=284) were included in the secondary analysis of CT-QFR's overall diagnostic performance **(Figure 1)**. Patients with conclusive ICA data (not fulfilling exclusion criteria V and VI) were included in the secondary intention-to-diagnose analysis (n=349).

Myocardial perfusion scintigraphy and cardiovascular magnetic resonance imaging

The non-invasive imaging (CMR and MPS) protocols were previously described in detail[5,6]. In short, an abnormal MPS scan was defined as (i) a summed difference score (SDS) ≥4 involving ≥2 contiguous segments (reversible), (ii) a summed resting score (SRS) ≥4 involving ≥2 contiguous segments (irreversible), and (iii) a combination of (i) and (ii) (mixed). MPS perfusion abnormalities were recalculated for a secondary analysis using the less stringent criteria defined as SSS >3 as applied in previous studies[17]. CMR abnormality was defined as subendocardial or transmural changes by stress imaging (reversible) or irreversible defects in ≥2 contiguous segments by late gadolinium enhancement imaging. MPS and CMR were analysed by independent core laboratories (Department of Nuclear Medicine & PET Centre, Aarhus University Hospital, Aarhus, Denmark, and Barts Heart Centre, Barts Health NHS Trust, London, United Kingdom).

Invasive coronary angiography

ICA was performed according to standard practice within four weeks following coronary

CTA. Invasive FFR was measured in lesions with 30-90% diameter stenosis (DS) using intravenous administration of adenosine (140 μg/kg/min). All ICA procedures were assessed with two-dimensional quantitative coronary angiography (2D-QCA) by an independent core laboratory (ClinFact, Leiden, the Netherlands). Patient-level haemodynamic obstructive disease was defined as (i) ≥1 stenosis with invasive FFR ≤0.80, (ii) ≥1 high-grade stenosis with visual >90% DS or (iii) ≥1 stenosis with 2D-QCA DS >50% if invasive FFR was not feasible. For vessel-level comparison of CT-QFR with invasive FFR as reference, invasive FFR ≤0.80 was used as diagnostic cut-off. Only lesions with 30-90% DS and measured wire-based FFR were included for vessel-level comparison.

Flow estimation using coronary CT angiography

In the hierarchical fractal-like cardiovascular system, volumetric flow and arterial volume were empirically measured in a ~3/4 power law and linear relationship with perfused myocardial mass, respectively[18], based on the flow-morphology relation in allometric scaling law[19]. Therefore, a 3/4 power law was finally applied in the function of estimating resting volumetric flow (Q) by using normal (reference) arterial volume (V).

$$Q \sim V^{\frac{3}{4}} \qquad (1\text{-}1)$$

The hyperaemic flow applied in CT-QFR computation was then computed from resting flow by using the following equation[20]:

$$HFV = 0.10 + 1.55*RFV - 0.93*RFV^2 \qquad (1\text{-}2)$$

in which HFV is hypaeremic flow velocity and RFV is resting flow velocity.

To obtain the reference arterial volume which was used for resting flow estimation, a bifurcation model was proposed to restore the normal lumen geometry. Previously reported bifurcation fractal laws revealed the relationship of lumen size among proximal main vessel, distal main vessel and branch, including the Murray and HK bifurcation laws derived from minimum energy hypothesis, an empirical fractal-like Finet model and an area-preservation-based model[21].

Besides the lumen size that has been widely applied, the bifurcation angle and distal resistance of each branch also contribute to the flow distribution. The current bifurcation model was therefore proposed **(Supplementary Figure 1)** by integrating the bifurcation angle and branch length into the diameter model.

Based on the flow-preservation rule, the following equation was available:

$$V_0 D_0^2 = V_1 D_1^2 + V_2 D_2^2 \quad (1\text{-}3)$$

in which V_0 is the flow velocity of the proximal main vessel, V_1 and V_2 are the flow velocity of two daughter vessels, D_0 is the reference diameter of the mother vessel, D_1 and D_2 are reference diameters of the two daughter vessels, respectively.

The contribution of bifurcation angle and branch length was embodied in the relationship of flow velocity in the branch and proximal main vessel.

$$V_1 = V_0 * (1 - e^{-\frac{\alpha_1 L_1}{\alpha_2 L_2}}) \quad (1\text{-}4)$$

$$V_2 = V_0 * (1 - e^{-\frac{\alpha_2 L_2}{\alpha_1 L_1}}) \quad (1\text{-}5)$$

in which α_1 is the bifurcation angle between the axis of the proximal main vessel and the axis of the daughter vessel at the ostia, L_1 is the branch length from the current branch origin to the most distal position, α_2 and L_2 are respective indices of the other daughter vessel **(Supplementary Figure 1)**. This bifurcation model allowed the determination of the reference diameter of the distal main vessel when the diameters of the proximal main segment and branch vessel were available. Each bifurcation model was computed in order from proximal to distal, with the diameter of the previous distal main vessel as that of the current proximal main vessel. Finally, a step-down reference lumen geometry was reconstructed along the main vessel, with step change crossing the bifurcations and gradual reduction in the most distal segment.

Supplementary Appendix 2. Results

Diagnostic performance of CT-QFR

The overall diagnostic accuracy for CT-QFR with ICA and invasive FFR as reference standard was 80.0% (95% CI: 74.8-84.3%). Additional diagnostic performance estimates are listed in **Table 3**. CT-QFR had a modest correlation (rho=0.51, p<0.001) and agreement (mean difference: 0.03±0.10) with invasive FFR on a per-vessel level **(Figure 2)**. Significant heteroscedasticity was observed with larger CT-QFR scatter for low invasive FFR values (p=0.003). **Supplementary Table 2** illustrates baseline demographics and procedural characteristics stratified according to CT-QFR and invasive FFR correspondence. Median Agatston calcium score was higher in patients with CT-QFR <0.80 and no haemodynamic disease by ICA and invasive FFR compared to patients with CT-QFR >0.80 and no haemodynamic disease by ICA and invasive FFR **(Supplementary Table 2)**. More patients had their lowest CT-QFR value in the 0.75-0.85 range for discordant results versus concordant results (47% [95% CI: 33-60] vs 19% [95% CI: 14-24]). Sensitivity was the highest for patients presenting with typical angina (86% [95% CI: 75-97]) and the lowest for patients presenting with non-anginal chest pain (47% [95% CI: 23-72]). **Supplementary Figure 3** illustrates the diagnostic performance for CT-QFR stratified by symptoms. On a per-vessel level, left main coronary artery or proximal left anterior descending artery stenosis tended to be associated with CT-QFR >0.80 and FFR ≤0.80 (p=0.08 for difference in occurrence among correspondence groups) **(Supplementary Table 2)**.

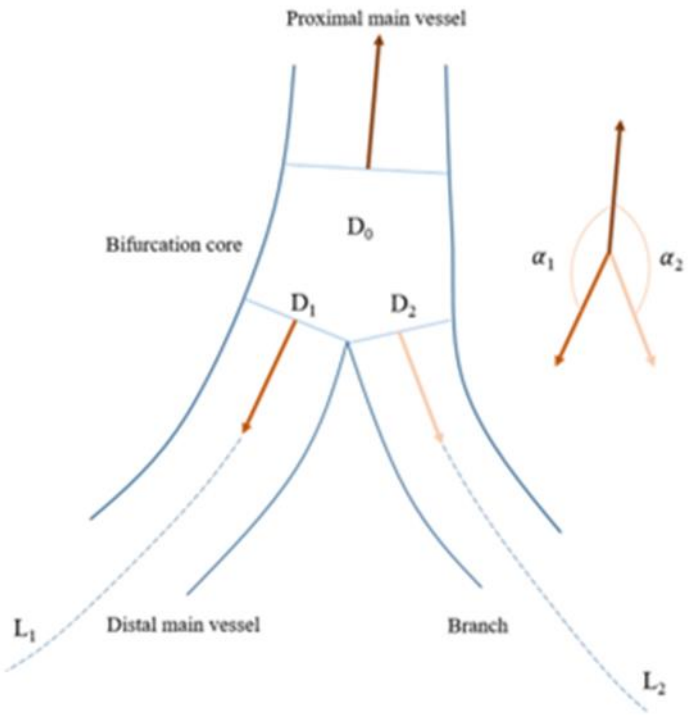

Supplementary Figure 1. A normal bifurcation model.

D0, D1 and D2 are reference diameters of the mother vessel and the two daughter vessels. α1, α2 and L1, L2 are the bifurcation angle and length of the two daughter branches, respectively.

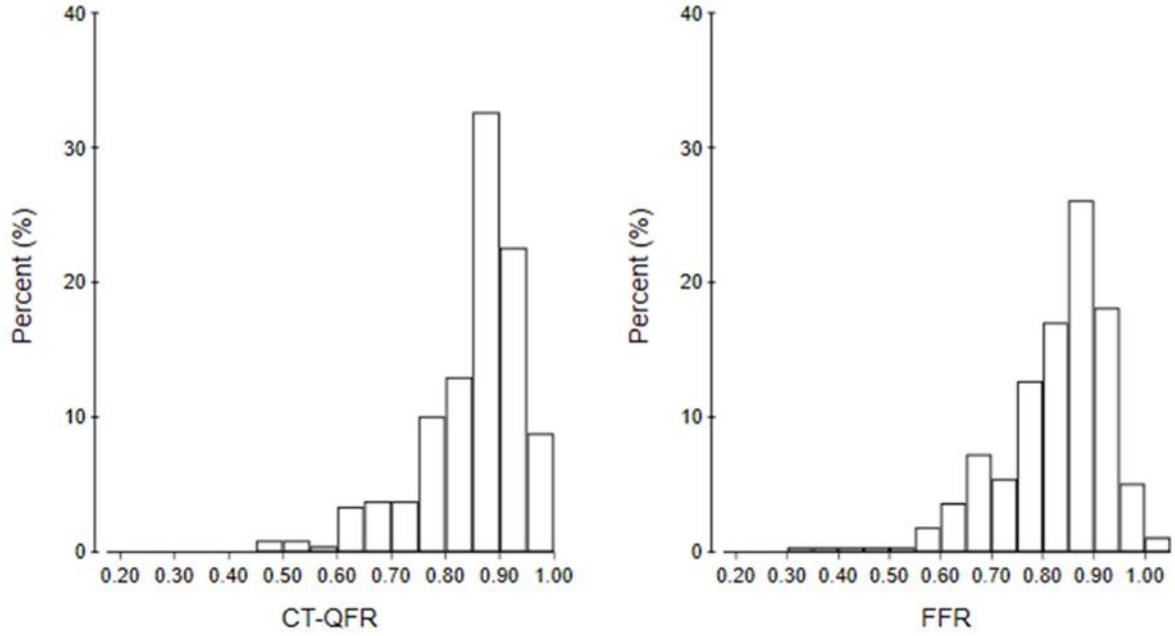

Supplementary Figure 2. Distribution of CT-QFR and FFR on a per-vessel level.

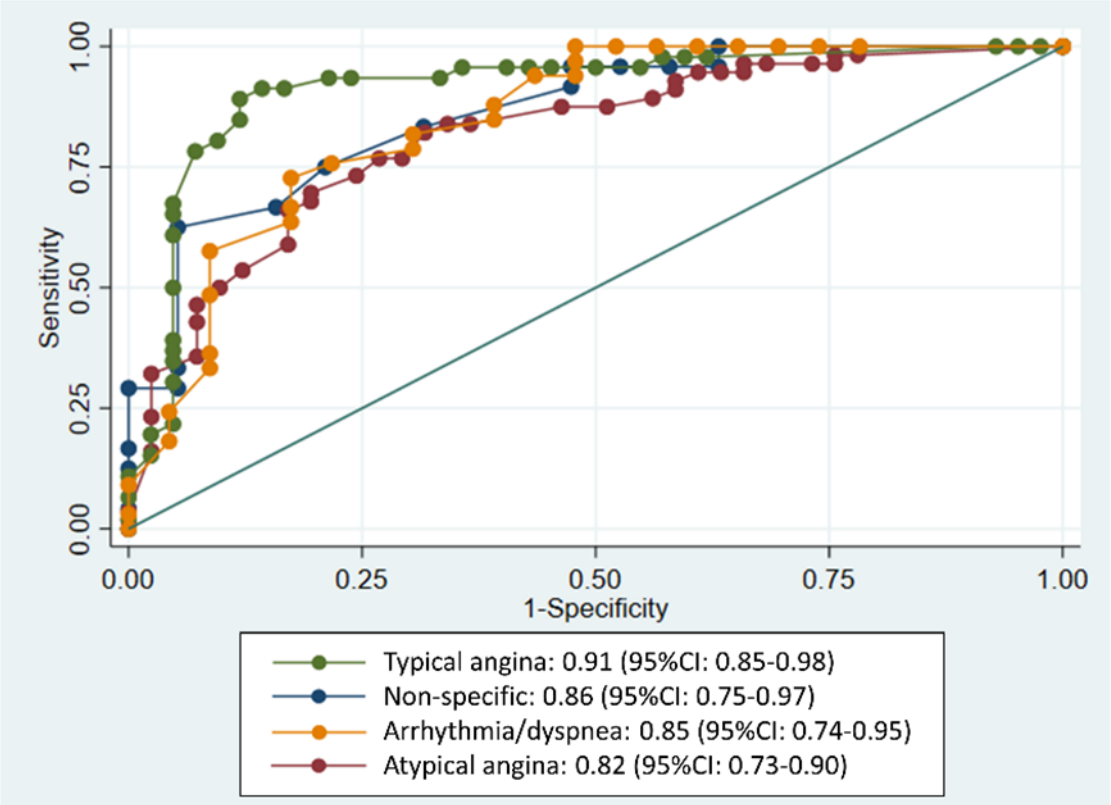

Supplementary Figure 3. Diagnostic performance of CT-QFR stratified by symptoms.

Supplementary Table 1. Comparison of clinical and procedural characteristics stratified by CT-QFR feasibility.

	CT-QFR feasible (n=284)	CT-QFR not feasible (n=61)	*p*-value
Demographics			
Age, years	60.7±8.2	62.3±8.1	0.15
Male	177 (62)	30 (49)	0.06
Body mass index, kg/m^2	27.2±4.1	26.9±4.4	0.63
Risk factors			
Current smoking	55 (19)	12 (20)	0.80
Hypertension	193 (68)	44 (72)	0.65
Hypercholesterolaemia	98 (35)	17 (28)	0.18
Diabetes	25 (9)	7 (12)	0.33
Family history of CAD	119 (42)	20 (33)	0.12
CCTA			
Heart rate, beats/min	56±7 (34-120)	61±8 (41-78)	<0.01
Agatston score	214 (63-585)	469 (118-1,005)	0.02
0	22 (8)	4 (7)	1.00
1-399	164 (58)	25 (41)	0.02
≥400	97 (34)	32 (53)	<0.01
Haemodynamic disease			
≥1 vessel with FFR ≤0.80	62 (22)	9 (15)	0.50
≥1 vessel with >90% DS	52 (18)	12 (20)	0.40
≥1 vessel with >50% DS QCA	11 (4)	1 (2)	0.69

Numbers are mean±SD or n (%).

CAD: coronary artery disease

Supplementary Table 2. Patient and procedural characteristics stratified by CT-QFR versus ICA/FFR correspondence.

Per-patient (n=284)					*p*-value
	Concordant	**Discordant**		**Concordant**	
	CT-QFR ≤0.80 & haemodynamic disease* (n=87)	**CT-FR >0.80 & haemodynamic disease* (n=38)**	**CT-QFR ≤0.80 & haemodynamic disease** (n=20)**	**CT-FR >0.80 & haemodynamic disease** (n=139)**	
Age, years	60±9	57±9	63±8	62±7	0.11
Male	65 (75)	23 (61)	13 (65)	76 (55)	0.03
Body mass index	27.2±4.4	27.1±4.1	27.0±4.8	27.2±3.8	0.41
Symptoms					0.56
Typical angina	36 (41)	6 (16)	4 (20)	42 (30)	
Atypical angina	28 (32)	13 (34)	10 (50)	46 (33)	
Dyspnoea or arrhythmia	14 (16)	9 (24)	5 (25)	28 (20)	
Non-anginal chest pain	9 (10)	10 (26)	1 (5)	23 (17)	
Hypertension	63 (72)	25 (66)	12 (60)	93 (67)	0.68
Diabetes	10 (12)	6 (16)	1 (5)	8 (6)	0.17
Agatston score	517 (142-999)	146 (42-316)	408 (169-1,068)	108 (25-337)	<0.01
CT-QFR 0.75-0.85	16 (18)	19 (50)	8 (40)	27 (19)	<0.01
Per-vessel with paired FFR and CT-QFR (n=239)					
	Concordant	**Discordant**		**Concordant**	
	CT-QFR ≤0.80 & FFR ≤0.80 (n=41)	**CT-FR >0.80 & FFR ≤0.80 (n=43)**	**CT-QFR ≤0.80 & FFR >0.80 (n=15)**	**CT-FR >0.80 & FFR >0.80 (n=140)**	
Lesion location					0.02
LMCA/prox LAD	4 (10)	8 (19)	0 (0)	10 (7)	
Mid/distal LAD	30 (73)	21 (49)	11 (73)	63 (45)	
LCx	3 (7)	5 (12)	1 (7)	37 (26)	
RCA	4 (10)	9 (21)	3 (20)	30 (21)	

Numbers are mean±SD, median (IQR) or n (%). * ≥1 stenoses with invasive FFR≤0.80, one or more high-grade stenosis with visual >90% DS or ≥1 stenoses with 2D-QCA DS >50% if invasive FFR was not feasible; **no epicardial disease. LAD: left anterior descending; LCx: left circumflex; LMCA: left main coronary artery; RCA: right coronary artery

Supplementary Table 3. Comparison of diagnostic performance estimates for CMR versus CT-QFR and MPS versus CT-QFR using revascularisation as reference standard.

	CT-QFR (n=284)	**CMR versus CT-QFR (n=113)**		***p*-value**	**MPS versus CT-QFR (n=118)**		***p*-value**
		CMR	*CT-QFR*		*MPS*	*CT-QFR*	
Accuracy	80.0 (74.9-84.3)	67.3 (58.5-76.0)	75.2 (67.1-83.3)	0.14	74.6 (67.0-83.0)	83.1 (76.2-90.0)	0.10
Sensitivity	74.3 (64.6-82.4)	37.1 (21.5-55.1)	60.0 (42.1-76.1)	0.06	43.6 (27.8-60.4)	84.6 (69.5-94.1)	<0.01
Specificity	82.5 (76.2-87.7)	80.8 (70.3-88.8)	82.1 (71.7-89.8)	0.82	89.9 (81.0-95.5)	82.3 (72.1-90.0)	0.18
PPV	70.1 (60.5-78.6)	46.4 (27.5-66.1)	60.0 (42.1-76.1)	0.17	68.0 (46.5-85.1)	70.2 (55.1-82.7)	0.82
NPV	85.3 (79.2-90.2)	74.1 (63.5-83.0)	82.1 (71.7-89.8)	0.06	76.3 (66.4-84.5)	91.5 (82.5-96.8)	0.04
LR (+)	4.25 (3.04-5.94)	1.93 (1.03-3.61)	3.34 (1.94-5.77)	0.17	4.30 (2.04-9.09)	4.77 (2.91-7.82)	0.82
LR (-)	0.31 (0.22-0.44)	0.78 (0.59-1.03)	0.49 (0.32-0.74)	0.06	0.63 (0.47-0.84)	0.19 (0.09-0.39)	<0.01
AUC	0.85 (0.80-0.89)	-	-		-	-	

Numbers are mean (95% CI).
AUC: area under the receiver operating curve; LR (-): negative likelihood ratio; LR (+): positive likelihood ratio; NPV: negative predictive value; PPV: positive predictive value

Supplementary Table 4. Diagnostic performance of MPS using SSS >3 as criteria for abnormality.

	MPS (n=118)
Accuracy	67.8 (59.2-76.3)
Sensitivity	39.6 (25.8-54.7)
Specificity	87.1 (77.0-93.9)
PPV	67.9 (47.6-84.1)
NPV	67.8 (57.1-77.2)
LR (+)	3.08 (1.52-6.22)
LR (-)	0.69 (0.54-0.89)

Numbers are mean (95% CI).
LR (-): negative likelihood ratio; LR (+): positive likelihood ratio; NPV: negative predictive value; PPV: positive predictive value

Supplementary Table 5. Diagnostic accuracy of CT-QFR, MPS and CMR stratified by type of perfusion defect.

Type of perfusion defect		Haemodynamic disease ICA/FFR			Accuracy CT-QFR	Accuracy MPS	Accuracy CMR
		FFR ≤0.80	High-grade stenosis (>90% DS)	QCA > 50% DS			
Reversible	40 (75)	13 (33)	11 (28)	0 (0)	88 (77-98)	60 (32-88)	60 (39-81)
Mixed	11 (21)	4 (36)	5 (45)	1 (9)			
Irreversible	2 (4)	1 (50)	1 (50)	0 (0)			

Diagnostic accuracy estimates were not added for mixed and irreversible defects given the low prevalence of these.
CMR: cardiovascular magnetic resonance; CT-QFR: CT-derived quantitative flow ratio; DS: percent diameter stenosis; FFR: fractional flow reserve; ICA: invasive coronary angiography; MPS: myocardial perfusion scintigraphy; QCA: quantitative coronary angiography

Supplementary Table 6. Patient-level 3*2 contingency tables with the intention to diagnose.

	Haemodynamic disease ICA/FFR		
CTA+CT-QFR	+	-	
+	87	20	107
Non-evaluable	25	40	65
-	38	139	177
	150	199	349

	Haemodynamic disease ICA/FFR		
MPS	+	-	
+	21	6	27
Non-evaluable	21	16	37
-	34	78	112
	76	100	176

	Haemodynamic disease ICA/FFR		
CMR	+	-	
+	23	13	36
Non-evaluable	18	11	29
-	33	75	108
	74	99	173

Supplementary Table 7. Comparison of diagnostic performance estimates for CMR versus CT-QFR and MPS versus CT-QFR with the intention to diagnose.

	CT-QFR (n=349)	**CMR vs CT-QFR (n=173)**			**MPS vs CT-QFR (n=176)**		
		CMR	*CT-QFR*	***p*-value**	*MPS*	*CT-QFR*	***p*-value**
Accuracy	65.8 (59.7-69.8)	56.7 (49.2-64.1)	62.4 (55.1-69.7)	0.320	56.3 (48.8-63.7)	67.0 (60.0-74.1)	0.034
Sensitivity	58.0 (49.7-66.0)	31.1 (20.8-42.9)	51.5 (39.4-63.1)	0.024	27.6 (18.0-39.1)	64.5 (52.7-75.1)	<0.001
Specificity	69.8 (63.0-76.1)	75.8 (66.1-83.8)	70.7 (60.7-79.4)	0.446	78.0 (68.8-85.7)	69.0 (59.0-77.9)	<0.001
PPV	59.2 (50.8-67.2)	48.9 (34.1-63.9)	56.7 (44.0-68.8)	0.339	48.8 (33.3-64.5)	61.3 (49.7-71.9)	0.099
NPV	68.8 (61.9-75.1)	59.5 (50.4-68.2)	66.0 (56.2-75.0)	0.100	58.6 (49.8-67.1)	71.9 (61.8-80.6)	<0.001
LR (+)	1.92 (1.50-2.47)	1.28 (0.79-2.08)	1.75 (1.20-2.56)	0.338	1.26 (0.75-2.11)	2.08 (1.49-2.91)	0.093
LR (-)	0.60 (0.49-0.74)	0.91 (0.75-1.10)	0.69 (0.53-0.90)	0.104	0.93 (0.78-1.10)	0.51 (0.37-0.72)	<0.001

Numbers are mean (95% CI).
LR (-): negative likelihood ratio; LR (+): positive likelihood ratio; NPV: negative predictive value; PPV: positive predictive value